

Electrohydrodynamic Mixing-Mediated Nanoprecipitation for Polymer Nanoparticle Synthesis

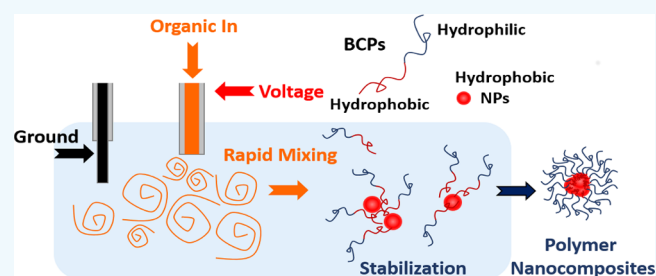
Kil Ho Lee,[†] Guolingzi Yang,[†] Barbara E. Wyslouzil,^{*,†,‡,||} and Jessica O. Winter^{*,†,§,||}

[†]William G. Lowrie Department of Chemical and Biomolecular Engineering, [‡]Department of Chemistry and Biochemistry, and [§]Department of Biomedical Engineering, The Ohio State University, 151 W. Woodruff Avenue, Columbus, Ohio 43210, United States

Supporting Information

ABSTRACT: As nanomaterials move toward commercial applications, methods of scalable, solution-based manufacturing of polymer nanoparticles are increasingly important. Flash nanoprecipitation (FNP) is a popular approach to producing relatively monodisperse NPs that encapsulate hydrophobic cargo with high efficiency. In conventional FNP, rapid turbulent mixing is generated by high velocity flows that may not be suitable for delicate or expensive cargo. Here, we developed an alternate approach to synthesize block copolymer (BCP) nanoparticles that relies on rapid mixing induced by electrohydrodynamics (EHD): EHD mixing (EM) mediated-nanoprecipitation (NP). For poly(caprolactone)-*b*-poly(ethylene oxide) (PCL-*b*-PEO) and poly(styrene)-*b*-PEO (PS-*b*-PEO) model polymers and over the range of conditions investigated, EM-NP yielded polymer NPs that were ~20 nm in diameter with polydispersity (standard deviation * mean⁻¹) of ~0.1 to 0.2. NP sizes were insensitive to changes in flow rate and BCP concentration but were slightly sensitive to changes in applied voltage. As voltage decreased the mean NP size and polydispersity remained unchanged but a small number of outlier worm-like micelles or larger spherical structures appeared. EM-NP was used to encapsulate hydrophobic cargos, including superparamagnetic iron oxide nanoparticles (SPIONs) or quantum dots (QDs), materials useful in biomedical imaging and cell separations. BCP nanocomposite size (~20 nm) and polydispersity remained relatively unchanged with hydrophobic cargo encapsulation; however, the tail of the distribution extended to larger particle sizes. Although BCP-QD composites synthesized via EM-NP demonstrated an ~20% decline in QD fluorescence in the first 24 h, they remained stable for the remaining 6 days of the study. Thus, EM-NP provides an important alternative to conventional FNP for generating monodisperse NPs that does not require high flow rates and that is superior to aerosol-mediated or sonication-mediated interfacial instability approaches. This process may enable commercial scale production of polymeric nanoparticles encapsulating delicate cargoes, such as quantum dot bioimaging agents.

KEYWORDS: block copolymer, nanoparticle, flash nanoprecipitation, nanomanufacturing, quantum dot, superparamagnetic iron oxide nanoparticle



INTRODUCTION

Polymer nanoparticles (NPs) and nanocomposites are critical components in a wide range of applications, ranging from bioimaging and drug delivery to energy harvesting and storage.^{1,2} Polymer NPs comprised of block copolymers (BCPs) (e.g., amphiphilic diblock³ and multiblock⁴) are particularly useful because of their high capacity to encapsulate relatively large hydrophobic cargoes (i.e., other NPs or drug molecules) and stabilize them in an aqueous environment.⁵ These nanocomposites can preserve the desired characteristics of the original hydrophobic constituents, while enhancing delivery and protecting against degradation. Furthermore, BCPs can be designed with a wide variety of “smart” characteristics, such that composite NPs can release their cargo or otherwise respond if triggered by pH, thermal, or optical excitation.⁶ However, many NP composites have only been synthesized in limited-scale, batch processes, often

yielding quantities far below those required for potential commercial use.⁷ Scaling up production, while maintaining high product quality, remains a challenge. Thus, it is often difficult to translate encouraging small scale results into commercial successes.

Standard synthesis methods for polymer NPs and nanocomposites are based on one of two fundamental mechanisms: kinetically driven encapsulation during nucleation and NP growth⁸ and thermodynamically driven self-assembly.⁵ Kinetic mechanisms have shown particular promise because they can encapsulate large amounts of hydrophobic cargo while maintaining narrow NP size distributions.^{9–11} In particular, the batch water addition (WA) method^{9,10} has been scaled up

Received: December 6, 2018

Accepted: March 18, 2019

Published: March 18, 2019

by Johnson and Prud'homme to yield BCP nanocarriers encapsulating therapeutics and inorganic nanoparticles via the flash nanoprecipitation (FNP) method.¹¹ This continuous nanomanufacturing process generates composite NPs via rapid precipitation of hydrophobic materials (the cargo) that are then stabilized by the coprecipitating amphiphilic block copolymers (BCPs). Conventional FNP is conducted in a high velocity environment (i.e., confined impinging jet mixer, multi-inlet vortex mixer) where the water-miscible organic solvent containing the BCP and hydrophobic cargo rapidly mixes with an antisolvent stream(s) (e.g., water).¹¹ The cargo and the BCPs supersaturate as the solvent quality is reduced during mixing, promoting precipitation of both components. Ideally, the nucleation and growth of the hydrophobic cargo exposed to a sudden change in solvent quality is arrested as the hydrophobic segments of the BCP stabilize the surface of the hydrophobic NP aggregates. Hence, the end product consists of hydrophobic cargo encapsulated in the hydrophobic region of the BCP, with the external, hydrophilic BCP block ensuring water-solubility. FNP has been utilized to produce polymer nanocomposites encapsulating inorganic NPs and drug molecules with encapsulation efficiencies of up to 99.9%.¹²

A fundamental requirement in FNP processes is rapid, turbulent mixing to achieve homogeneous kinetics; mixing must be sufficiently rapid that the solution is homogeneous and the nucleation and growth kinetics are uniform throughout. Thus, most devices rely on high flow rates (up to mL min⁻¹ scale) to achieve efficient turbulent mixing. As a consequence, more controlled, lower volume synthesis can be difficult to achieve when only a limited amount of cargo is available, although progress has been made in the form of a simplified, hand operated, confined impinging jet mixer with dilution.¹³ Some of these challenges can be addressed using microfluidic platforms¹⁴ or membrane dispersion devices,¹⁵ but incorporating such devices into large manufacturing processes may require specialized fabrication techniques. There remains a strong need to develop simple, yet scalable FNP platforms that are not directly dependent on high flow rates or high fluid velocities.

Here, we employ rapid electrohydrodynamic (EHD) mixing¹⁶ to develop an nanoprecipitation process (EM-NP) that complements the conventional jet mixing approach. In the EM-NP configuration, a liquid with low electrical conductivity (i.e., tetrahydrofuran, THF) is pumped into a miscible liquid that has a relatively higher, but still low, electrical conductivity (i.e., distilled water). The presence of an electric field can both induce motion of the charge carriers within the more conductive liquid, leading to bulk fluid flow, as well as directly disrupt the interface between the two fluids. Both effects increase with the strength of the electric field and under a strong enough field, lead to rapid turbulent mixing of the two liquids. Using EM-NP, we demonstrate synthesis of PCL-*b*-PEO and PS-*b*-PEO NPs and characterize the effect of applied voltage, flow rate, and BCP concentration on the size and polydispersity of the NPs. We also encapsulate inorganic NPs, including luminescent semiconducting quantum dots (QDs) and superparamagnetic iron oxide nanoparticles (SPIONs), in PS-*b*-PEO BCPs. QDs in particular were chosen because of their high sensitivity to the external environment,¹⁷ thus QD fluorescence can serve as an indicator of EM-NP ability to process delicate cargo.

EXPERIMENTAL SECTION

Materials. Poly(ϵ -caprolactone-*b*-ethylene oxide) (PCL 6 kDa/PEO 5 kDa) and poly(styrene-*b*-ethylene oxide) (PS 9.5 kDa/PEO 18.0 kDa) with carboxylic acid termination were purchased from Polymer Source (Montreal, Canada). Hydrophobic QDs with octadecylamine ligands (particle size = 5 nm, λ_{em} = 600 nm) and hydrophobic SPIONs with oleic acid ligands (particle size = 5 nm) were purchased from Ocean NanoTech (San Diego, CA). Rhodamine 6G was purchased from ThermoFisher Scientific. Hamilton metal hub blunt point needles (27 gauge, 410 μ m o.d.; 210 μ m i.d.) and glass luer lock syringes (1 mL) were purchased from ThermoFisher Scientific. Polytetrafluoroethylene heat shrink tubing (30 gauge, 0.006 in. wall, shrink ratio 2:1) was purchased from Component Supply company (Lakeland, FL). For centrifugal filtration, Amicon Ultra centrifugal filter units (pore size: 100 kDa MWCO) were purchased from Sigma-Aldrich.

Polymer NP and Nanocomposite Synthesis via EM-NP. Polymer NPs and nanocomposites were synthesized using the same EM-NP setup (Figure S1). The electro spray needle was a 27 gauge (410 μ m o.d.; 210 μ m i.d.) blunt stainless steel capillary insulated to the tip with PTFE heat shrink tubing, and the grounding electrode was a stainless steel wire partially insulated with PTFE heat shrink tubing. The needle and the grounding electrode were positioned in the continuous phase (i.e., distilled water in a 15 mL glass vial), with the electro spray needle located \sim 1 cm below the surface and the grounding electrode \sim 1 cm away from the electro spray needle. A high voltage supply applied up to -2.5 kV across the grounding electrode and the electro spray needle. The organic phase was delivered to the electro spray needle via a syringe pump, and rapid mixing of the two fluids ensued as the applied voltage increased. Unless specifically noted, the flow rate used was 12.7 mL h⁻¹ and the applied voltage was -2500 V.

The composition of the organic phase varied depending on the type of product synthesized. For PCL-*b*-PEO and PS-*b*-PEO NPs, the stock polymer solution (10, 20, or 40 mg mL⁻¹, 200 μ L) in THF was added to 200 μ L of THF. For QD- and SPION-loaded PS-*b*-PEO NPs, the organic phase consisted of PS-*b*-PEO (10 mg mL⁻¹, 200 μ L) and QD (1.75 mg mL⁻¹, 200 μ L) or SPIONs (0.5 mg mL⁻¹, 200 μ L) in THF, respectively. In all cases, half of the total 400 μ L organic phase was mixed into 10 mL distilled water. NPs and nanocomposites were purified within 5 min of initial synthesis via centrifugal filtration (4000 rpm, 15 min) to remove excess THF. Centrifugal filtration was repeated 3 times with 3 mL of distilled water. After purification, \sim 200 μ L of purified product was retrieved by adding 800 μ L of distilled water. For all experiments, samples were synthesized and analyzed in triplicate.

Characterization of NP and Nanocomposite Size and Polydispersity. Transmission electron microscopy (TEM) was used to determine the size of the polymer NPs and composites. Briefly, a PELCO easiGlow Glow Discharge Cleaning System was used to clean TEM grids prior to NP deposition. This step aids adhesion of the samples by making the surface more hydrophilic. Then, 12.5 μ L sample droplets were pipetted onto a silicone pad over which the TEM grid was inverted for 5 min. Excess sample was then slowly wicked away using filter paper. Negative staining was performed using 1% uranyl acetate dissolved in distilled water. TEM images were collected using an FEI Tecnai G2 Bio Twin TEM at 80 kV.

Particle size and distribution parameters were obtained by analyzing TEM images using ImageJ software (available from NIH). The Feret length (L_F), the longest distance from any two points, was used as a characteristic length representing NP diameter. Size measurements were collected for each of the triplicate experiments and pooled. The total number of particles counted per experimental condition ranged from 400 to 7500 particles. Minimum and maximum particle sizes were obtained for each sample using MATLAB (MathWorks & Simulink, Natick, MA, U.S.A.). Size histograms were plotted using SigmaPlot (Systat Software Inc., San Jose, CA, U.S.A.), and size distributions were fit to log-normal distributions.

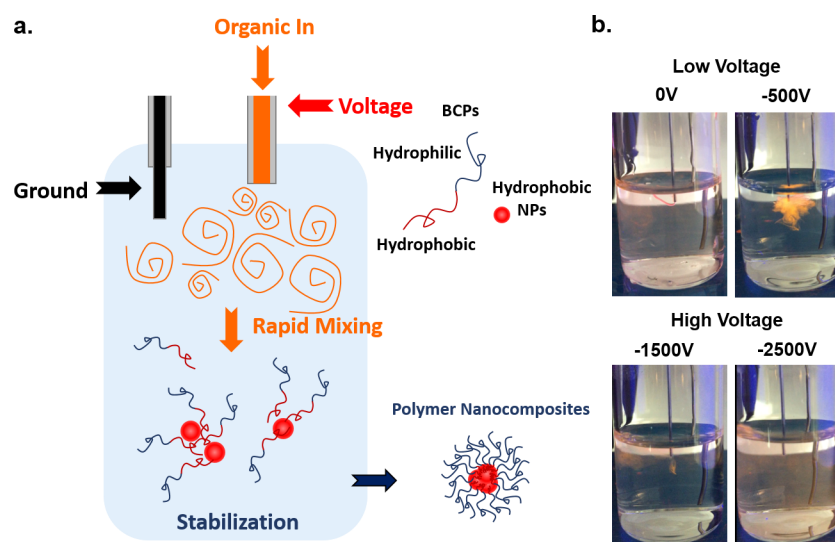


Figure 1. (a) Schematic of EHD mixing-mediated nanoprecipitation (EM-NP), and (b) EHD mixing of THF containing rhodamine 6G dye (orange) and water at a fixed liquid flow rate and different voltages. Mixing increases rapidly with increasing voltage.

Mode, mean, and geometric standard deviation were then extracted from the fit parameters. Lognormal distributions and fits for each pooled experiment (Figures S2–S5), as well as detailed descriptions of the method used to extract mean and standard deviation from the fit parameters are given in the Supporting Information.

For one set of experimental conditions, hydrodynamic diameter was additionally determined using dynamic light scattering (DLS) (BI 200-SM, Brookhaven Instruments Corp.). The average count rate was between 100 and 200 kilocounts per second, and light was collected at a 90° angle.

QD Fluorescence Intensity. Fluorescence intensity of QD-loaded PS-*b*-PEO composites was evaluated using a Photon Technology International (PTI)-810 fluorometer (excitation = 350 nm, lamp power = 75 W, detector voltage = 1100 V). Purified QD-loaded PS-*b*-PEO composites were too concentrated to measure directly. Hence, measurements were conducted on the total product (~200 μL) diluted in 5 mL of distilled water.

RESULTS AND DISCUSSION

EHD-Enhanced Mixing of a Water-Miscible Organic Liquid in Water. One of the most well-known applications of electrostatic forces in flow involves spraying a conductive fluid into a nonconductive fluid (C-in-N system) in the presence of an electric field.^{18,19} In this traditional electro spray approach, the voltage applied at the interface between the two fluids induces electric stresses that deform the interface yielding a number of different spray modes.²⁰ One of the most widely used is the cone-jet mode, in which the applied electric stresses overcome the surface tension of the fluid interface to yield a conical jet, known as a Taylor cone.^{21–24} The narrow jet of fluid emitted from the tip of the cone then breaks up to create a fine aerosol.

Although not as widely known, electric fields can also be used to disperse an immiscible nonconductive fluid inside a more conductive one^{16,25–29} (N-in-C system), yielding, for example, fine dispersions of bubbles or oil droplets in water. More recently, electrically induced mixing of two miscible fluids (Figure 1a) has also been explored as an alternative to flow rate dependent turbulent mixing, to produce inorganic nanoparticles as small as 240 nm.¹⁶ In all cases, dispersion and mixing efficiency increase with the strength of the electric field. Although “inverse” electro spray is not as well understood as

traditional electro spray, and both theoretical^{30–32} and experimental^{16,33–35} studies continue to investigate the relevant physics, two key phenomena have been identified as important to both droplet production and mixing. The first phenomenon is charge carrier migration through the leaky dielectric fluid from the injection point (electrode) toward the ground. Near the electrode, where the electric charge is highest, charge migration results in the electroconvection of the fluid that intensifies as the strength of electric field increases (Figure 1).³² Local velocities as high as 100 mm s⁻¹ have been measured 2 mm from the tip of the injection needle.³⁶ The second phenomenon is the disruption of the interface itself by the electrical stresses that further enhances dispersion and mixing.³⁶

In this work, we adopted the EHD mixing technique to build a simple platform for rapidly mixing a nonconductive, water-miscible, organic liquid (i.e., THF), containing polymers and other hydrophobic compounds, into distilled water. To the best of our knowledge, EHD mixing-mediated nanoprecipitation (EM-NP) has not been applied to systems involving self-assembly such as BCP micelles or nanocomposites (Figure 1a). EM-NP therefore presents an attractive option for nanoprecipitation polymer processing in which mixing intensity is not solely dependent on flow rate.

One challenge in achieving and maintaining an electric field in an N-in-C system is that the electrified needle and the grounding electrode are both in contact with the more conductive fluid. Applying a high voltage to the needle can, therefore, generate a short circuit unless the needle is well insulated.^{26,29} In earlier work, this was done by embedding the needle in glass or in a ceramic housing, but in this work, we insulated the needle by encasing it in PTFE heat shrink tubing. As an initial proof of concept, and to visualize mixing of the injected liquid, we pumped THF containing a fluorescence dye (i.e., Rhodamine 6G) into distilled water at a constant flow rate (12.7 mL h⁻¹) and varied the voltage (Figure 1b) in the absence of nanoparticle forming species (e.g., polymers, quantum dots). In the absence of an applied voltage the dye stream appears as an orange ribbon inside the aqueous phase that rises to the surface, suggesting there is little mixing between the less dense THF-dye mixture and the water. Applying a relatively

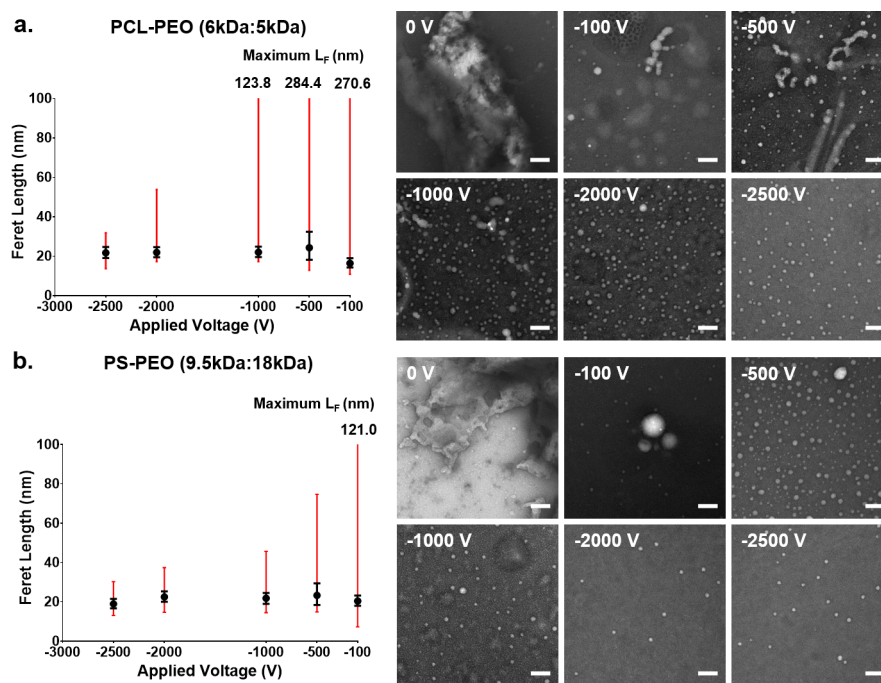


Figure 2. TEM analysis of (a) PCL-*b*-PEO and (b) PS-*b*-PEO NPs synthesized via EM-NP at various voltages. The black symbols and lines correspond to the mean ($\langle L_F \rangle$) and the particle size range that contains 68% of the particles, respectively. The red line joins the maximum and minimum sizes observed. TEM scale bar = 100 nm.

low voltage (-500 V) results in weak dispersion of the organic stream, biased in the direction of the ground wire, whereas increasing the voltage further to -1500 V results in more vigorous mixing. The stream exiting the needle also becomes less visible, and the aqueous phase quickly changes color as the organic phase rapidly disperses. At the maximum voltage tested, -2500 V, the organic phase exiting the needle is not visible because dispersion is too rapid. This finding is consistent with previous EHD micromixing reports that investigated mixing intensity is a function of the applied voltage.¹⁶

Effect of EM-NP Operating Parameters on BCP NP Morphology. Applied Voltage. To demonstrate that BCP NPs can be produced via EM-NP and to evaluate the effect of applied voltage on the morphology of the NPs generated, we mixed THF containing BCP into water at various voltages (0, -100 , -500 , -1000 , -2000 , and -2500 V). The size distributions of the resultant products were characterized using TEM. Two BCPs were studied: PCL_{6.0 kDa}-*b*-PEO_{5.0 kDa},³⁷ for direct comparison with prior FNP work by Prud'homme,³⁷ and PS_{9.5 kDa}-*b*-PEO_{18.0 kDa},³⁸ for direct comparison with BCP NPs produced in our previous work via sonication³⁸ and coaxial electrospray.²¹ The polymer concentrations in the organic stream were comparable with the work of Prud'homme (i.e., 10 mg mL⁻¹ for PCL-*b*-PEO) and our previous work (5 mg mL⁻¹ for PS-*b*-PEO), respectively.

Under the control conditions of 0 V (no applied voltage), both PCL-*b*-PEO and PS-*b*-PEO BCPs formed large agglomerates (Figure 2) without a well-defined morphology, and, thus, these data were omitted from further size analysis. When voltage was applied, structures consistent with BCP NPs were formed (Figure 2, Table S1). These structures were characterized with respect to L_F . The resulting histograms were then fit to log-normal size distributions. For both BCPs, the number mean L_F , $\langle L_F \rangle$, ranged from ~ 16 to 24 nm regardless

of the applied voltage (i.e., -100 to -2500 V). Similarly, the widths of the particle size distributions, defined such that 68% of the particles lie within this distance of $\langle L_F \rangle$, were between ~ 2 and 8 nm. These results suggest that both $\langle L_F \rangle$ and polydispersity are only weakly dependent on voltage (Table S1). In contrast, the maximum L_F observed (red bars) declined with increasing voltage, suggesting fewer, large particle outliers in the distribution; and accordingly, the number of particles with $\langle L_F \rangle > 50$ nm declined from 5.3% (PCL-*b*-PEO) and 1.4% (PS-*b*-PEO) at -100 V to 0% with increasing voltage (Figure S2). For PCL-*b*-PEO, TEM images demonstrated that increasing voltage reduced the number of worm-like NPs formed (e.g., compare, for example, -100 and -500 to -2500 V) and favored the spherical micelle morphology. For PS-*b*-PEO, increasing voltage also favored spherical structures; however, lower voltages resulted in large circular particles as opposed to worm-like micelles.

The success of FNP depends on three time scales: mixing time (τ_{mix}), nucleation and growth time for the encapsulants (τ_{ng}), and polymer aggregation time (τ_{agg}). Two criteria must be met to obtain highly monodisperse particles and high encapsulation efficiency. The first criterion involves τ_{mix} and τ_{agg} and can be cast in terms of the Dämkohler number, $Da = \tau_{\text{mix}}/\tau_{\text{agg}}$. Three mixing regimes are identified: (i) $Da \geq 1$, slow mixing results in inhomogeneous particle formation kinetics, (ii) $Da = 1$, a transition region, and (iii) $Da < 1$, rapid mixing establishes a uniform solution and homogeneous particle formation kinetics. The second criterion involves τ_{ng} and τ_{agg} . For effective stabilization, or encapsulation, of the growing hydrophobic encapsulant aggregates these times scales need to be approximately equal.³⁹ In a conventional FNP process, τ_{mix} is a function of the flow rates and the dimensions of the mixer used. Because of the complexity of the EHD system, τ_{mix} is not readily determined, but decreasing the voltage clearly decreases mixing intensity (Figure 1) and increases Da . Thus, changes in

nanoparticle size and morphology can be used as surrogates for changes in τ_{mix} .

EM-NP results (Figure 2) are consistent with the work of Johnson and Prud'homme,⁸ who found that, in the homogeneous kinetics regime, particle diameter is insensitive to flow rates. However, these authors also reported that, when flow rate decreases so that $Da > 1$, the average particle size increases. In contrast, in the current EM-NP design, the mean size is unaffected down to the lowest applied voltage (i.e., -100 V) investigated. Instead, as the voltage decreases, the tail of the size distribution extends to larger particle sizes. Nevertheless, the number of large particles is too low to greatly affect the mean and polydispersity derived from fits to the data. For example, for PCL-*b*-PEO NPs synthesized at -100 V, the sample with the largest fraction of large particles, $\langle L_F \rangle$ calculated including all particle sizes was 21.9 nm, $\langle L_F \rangle$ calculated including only those below 50 nm was 18.2 nm. Only under the control conditions (0 V), where τ_{mix} and Da are maximized and primarily a function of the flow rate of the entering liquid, were large, ill-defined aggregates observed. Experiments between 0 and -100 V would be expected to yield the transition to a regime where NP size depends strongly on voltage, similar to the shifts observed with flow rate in traditional FNP. Thus, these data establish that applied voltage can modulate τ_{mix} and suggest that in the current setup voltages as low as -100 V are sufficient to establish homogeneous kinetics.

Organic Phase Flow Rates. To determine the sensitivity of EM-NP to flow rate, a crucial variable in standard FNP configurations, we varied the organic phase flow rate (2.5, 5, 10, 12.7 mL h⁻¹) at a constant voltage (-2500 V) using the same polymer concentration as above and evaluated the effect on NP morphology. It should be noted that the flow rates used in this experiment were much lower than those used by Johnson and Prud'homme (organic 12 mL min⁻¹, aqueous 40 mL min⁻¹) and were limited by the throughput of the syringe pump employed. As in the voltage study, neither $\langle L_F \rangle$ nor polydispersity were strong functions of the organic phase flow rate (Figure 3 and Table S2). For PCL-*b*-PEO, the largest $\langle L_F \rangle$ (i.e., 29.8 nm) was obtained at the lowest flow rate, 2.5 mL h⁻¹. For PS-*b*-PEO, the largest $\langle L_F \rangle$ (i.e., 22.8) was obtained at 5.0 mL h⁻¹. There were also no trends observed in the minimum or maximum values. Thus, although the flow rates tested, between 2.5 and 12.7 mL h⁻¹, only varied by a factor of 4, it is reasonable to conclude that the success of EM-NP depends more strongly on the applied voltage than on the flow rate.

BCP Concentrations. One caveat to the observations above is that this version of EM-NP is a semicontinuous process rather than a fully continuous process as typically used in FNP. Thus, it is possible that temporal changes in the BCP concentration in the solution could affect NP size and morphology. To evaluate this possibility, we produced PCL-*b*-PEO and PS-*b*-PEO NPs at constant flow rate (12.7 mL h⁻¹) and voltage (-2500 V) but varied the BCP concentrations in the organic solution. Concentrations of 5, 10, and 20 mg mL⁻¹ were used, because these concentrations include the standard conditions of 10 mg mL⁻¹ for PCL-*b*-PEO and 5 mg mL⁻¹ for PS-*b*-PEO used above.

For both BCPs, increasing BCP concentration had a negligible effect on mean $\langle L_F \rangle$ as well as the width of the particle distribution (Figure 4 and Table S3). No trends with BCP concentration were observed. For PCL-*b*-PEO, the largest

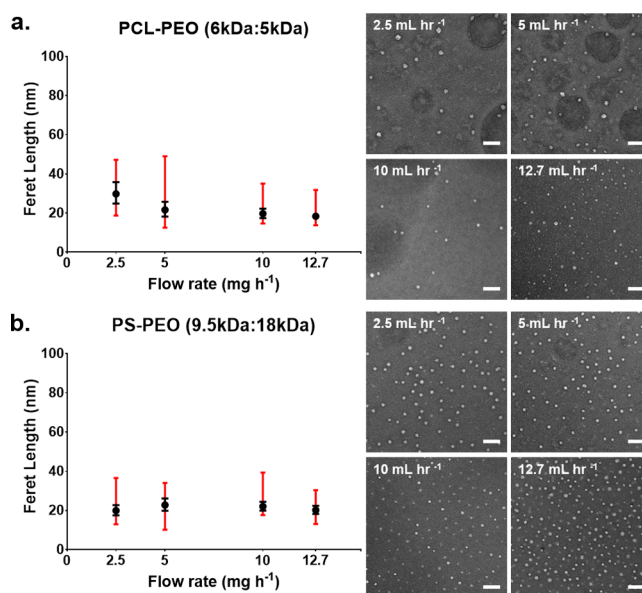


Figure 3. TEM analysis of (a) PCL-*b*-PEO and (b) PS-*b*-PEO NPs synthesized at various organic phase flow rates at a constant voltage (-2500 V) and polymer concentration. The black symbols and lines correspond to mean $\langle L_F \rangle$ and the particle size range that contains 68% of the particles, respectively. The red line joins the maximum and minimum sizes observed. TEM scale bar = 100 nm.

mean $\langle L_F \rangle$ occurred at a concentration of 5 mg mL⁻¹ (20.2 nm), whereas for PS-*b*-PEO, the largest mean $\langle L_F \rangle$ occurred at 20 mg mL⁻¹ (20.7 nm). Nor were there any specific trends for the minimum or maximum values observed across BCP concentrations. In their FNP studies, Johnson and Prud'homme also found that the NP size is independent of BCP concentration as long as homogeneous kinetics are obtained ($Da \leq 1$).⁸ Although the range of BCPs investigated is still limited, our results to date suggest that, with the exception of the control experiment (0 V), homogeneous kinetics were achieved under all conditions investigated, and that EM-NP is relatively insensitive to both flow rate and BCP concentration changes. It is possible that concentration dependence may emerge with other polymers, particularly if they can undergo postsynthetic Ostwald ripening.⁴⁰

Comparison to Other Scalable Nanomanufacturing Platforms. Selected EM-NP studies used the same polymers at comparable concentrations to other nanomanufacturing processes reported in the literature, in particular multi-inlet vortex mixer (MIVM)-mediated FNP of Prud'homme and co-workers,³⁷ and our previous results using sonication⁴¹ and coaxial electrospray⁴² mediated self-assembly. Thus, a direct comparison of the results should be reasonably straightforward.

For PCL-*b*-PEO (Table 1), EM-NP produced significantly smaller NPs than MIVM, ~ 18 nm versus 50 nm, although particle distribution widths were approximately the same. Polydispersity was, therefore, twice as high for particles made with EM-NP versus MIVM. Possible reasons for this size difference include (1) the size characterization technique, (2) the change in solvent quality that drives particle formation, and (3) the mechanism of inducing rapid mixing.

Prud'homme and co-workers used dynamic light scattering (DLS) to obtain hydrodynamic diameters of particles in solution, whereas we used TEM to obtain $\langle L_F \rangle$ of dried particles on a TEM grid. Our TEM results are, however, confirmed by DLS measurements (Figure S6). For PCL-*b*-

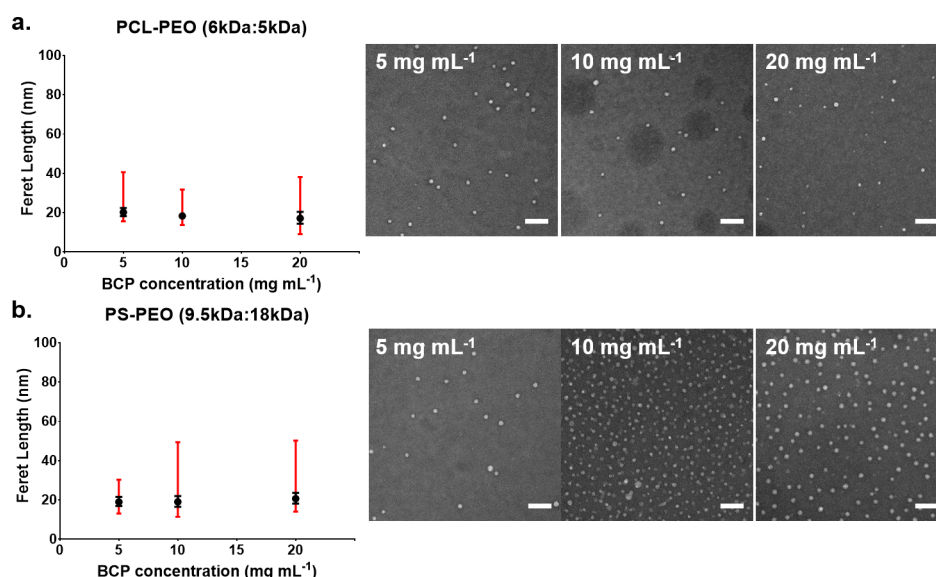


Figure 4. TEM analysis of (a) PCL-*b*-PEO and (b) PS-*b*-PEO NPs synthesized via EM-NP at various BCP concentrations in THF at a constant flow rate (12.7 mL h⁻¹) and voltage (-2500 V). The black symbols and lines correspond to mean (L_F) and the particle size range that contains 68% of the particles, respectively. The red line joins the maximum and minimum sizes observed. TEM scale bar = 100 nm.

Table 1. Size Comparison of PCL-*b*-PEO NPs Synthesized with Different Processes^a

	BCP conc in THF (mg mL ⁻¹)	mean L_F (nm)	PD/PD _{eff}
MIVM ³⁷	11	50 ± 2.0	0.04
EM-NP	10	18.3 ^{+1.6} _{-1.5}	0.08

^a L_F = Feret length. +, -: the interval defined by the upper and lower bounds on $\langle L_F \rangle$ contains 68% of the particles. PD_{eff} = $\sqrt{(+dev)(-dev)}/\langle L_F \rangle$

PEO NPs (BCP concentration: 10 mg mL⁻¹ in THF) DLS yielded an average hydrodynamic diameter of 24.1 nm, slightly larger than, but highly consistent with, the dried particle diameter measured by TEM (18.3 nm). Therefore, size characterization technique cannot explain the observed size difference for PCL-*b*-PEO NPs produced by the two techniques.

Prud'homme and co-workers reported that NP size is insensitive to BCP concentration once homogeneous kinetics are obtained⁴³ but that the final size NP does depend on the change in solvent quality, particularly the rate of change and the magnitude of the change.⁸ In particular, experiments showed that NP size increased with the organic content of the final mixed stream,⁸ and molecular dynamics (MD) simulations found that particle size decreased with an increase in the rate of solvent quality change.⁴⁴ In the MIVM experiments reported,³⁷ the BCP and THF concentrations in the final mixture are both about an order of magnitude greater (organic/aqueous ~0.3 v/v) than in the EM-NP process

(organic/aqueous ~0.02 v/v). Thus, if mixing times are comparable both the magnitude of the solvent quality change and the rate at which it occurred should be much greater in the current EM-NP experiments than in the MIVM experiments. Both effects should lead to smaller particles and in that sense our results are consistent with the work of Prud'homme and co-workers.^{8,44} These results are also consistent with basic ideas from nucleation literature, which suggest that higher saturations lead to more rapid particle formation and smaller particle size.

Finally, a major difference between EM-NP and MIVM is the mechanism of inducing rapid mixing—EHD flow around the nozzle tip and field induced instability at the interface versus turbulence throughout the flow. It is possible the electric field established during EM-NP could affect the final particle size. Masnky and co-workers, for example, demonstrated that in thin films of poly(styrene-*b*-methyl methacrylate), or PS-*b*-PMMA, alignment follows the electric field lines driven by the difference in the dielectric properties of the polymer blocks.⁴⁵ Understanding the effect the electric field may have on BCP aggregation to form NPs during EM-NP is beyond the scope of this paper. On the basis of the insensitivity of particle size to a 25-fold increase in voltage, however, any effect is likely small.

For PS-*b*-PEO micelles (Table 2), the current results using EM-NP were compared to NP formation via sonication⁴¹ and Aero-IS coaxial electrospray.⁴² In the latter two processes, BCP self-assembly proceeded via the interfacial instability mechanism from an oil-in-water emulsion, and micelle assembly was

Table 2. Size Comparison of PS-*b*-PEO NPs Made with Different Synthesis Processes^a

	5 mg mL ⁻¹		10 mg mL ⁻¹		20 mg mL ⁻¹	
	mean L_F (nm)	PD or PD _{eff}	mean L_F (nm)	PD or PD _{eff}	mean L_F (nm)	PD or PD _{eff}
sonication ⁴²	N/A	N/A	44.0 ± 10.3	0.23	53.2 ± 14.8	0.28
coaxial electrospray ⁴²	49 ± 11.0	0.22	51.5 ± 13.5	0.26	73.3 ± 14.7	0.20
EM-NP	19.0 ^{+2.6} _{-2.3}	0.13	19.0 ^{+3.0} _{-2.6}	0.14	20.7 ^{+3.0} _{-2.6}	0.13

^a L_F = Feret length. +, -: the interval defined by the upper and lower bounds on $\langle L_F \rangle$ contains 68% of the particles. PD_{eff} = $\sqrt{(+dev)(-dev)}/\langle L_F \rangle$

a thermodynamically driven process.⁴⁶ PS-*b*-PEO NPs formed using Aero-IS and sonication were similar in size and polydispersity but distinctly larger in size and with higher polydispersity than NPs synthesized by EM-NP. Unlike the rapid formation of NPs in FNP, the self-assembly of BCPs in the interfacial instability process takes longer (hours versus seconds), as BCPs organize to form the most thermodynamically stable configuration characterized by the critical micelle concentration (CMC).⁴⁶ Particle size is determined by the CMC, rather than kinetic-trapping, and polydispersity is larger as slow particle growth by chain insertion and aggregate fusion leads to a broadening of the size distribution. Thus, compared to thermodynamic self-assembly approaches, EM-NP yields smaller NP size with superior polydispersity. Lastly, Aero-IS- and sonication-mediated BCP assembly both led to elongated structures (i.e., ellipsoidal and wormlike) as the BCP concentration in the organic phase increased, and the morphology shift was higher in Aero-IS than in sonication. In EM-NP, in the homogeneous kinetics regime, BCP concentration showed negligible effect on the particle size and the morphology.

Overall, NPs synthesized via EM-NP were smaller than NPs synthesized via other manufacturing techniques. The particle size difference found in EM-NP versus MIVM is qualitatively consistent with changes in solvent quality. Thus, altering the solvent quality by dispersing the THF/BCP solution into a water mixture already containing THF may offer a way to control the particle size via EM-NP. Comparing EM-NP to thermodynamically driven techniques, suggests that EM-NP is suitable for synthesizing smaller, more monodisperse NPs, whereas Aero-IS and sonication may be desired for producing micelles with higher order morphologies.

Synthesis of BCP Nanocomposites Encapsulating Inorganic NPs via EM-NP. The ability of BCP micelles and NPs to encapsulate hydrophobic cargo is a key feature of their application, and FNP in an MIVM can do so with high efficiency.³⁷ We therefore conducted EM-NP experiments using THF containing PS-*b*-PEO BCP and either semi-conducting fluorescent quantum dots (QDs) or superparamagnetic iron oxide nanoparticles (SPIONs) as model cargoes. To minimize τ_{mix} and promote homogeneous kinetics, the organic phase flow rate and the applied voltage were held constant at 12.7 mL h⁻¹ and -2500 V, as in our previous experiments.

To evaluate the ability of resultant nanocomposites to encapsulate these cargoes, several tests were performed. As a first test of encapsulation efficiency, the resultant NP solutions were centrifuged immediately after particle formation to identify any aggregates associated with unencapsulated QDs or SPIONs. No pellets were formed, at least at these encapsulant concentrations. We also measured the fluorescence intensity of the filtered supernatant to detect any unencapsulated QDs, but no fluorescence was observed (Figure S8). Next, we evaluated nanocomposite structures via TEM. TEM images showed that the products contained both empty PS-*b*-PEO NPs and composites encapsulating inorganic NPs (Figure 5, inset). For consistency, loaded and empty PS-*b*-PEO nanocomposite sizes were evaluated separately (Figure 5, Table 3).

For PS-*b*-PEO composites encapsulating QDs, $\langle L_F \rangle$ was ~ 2 nm larger than $\langle L_F \rangle$ for PS-*b*-PEO composites encapsulating SPIONs. Empty micelles in the same samples had $\langle L_F \rangle$ values of 18.1 nm for PS-*b*-PEO with QDs and 17.0 nm for PS-*b*-PEO

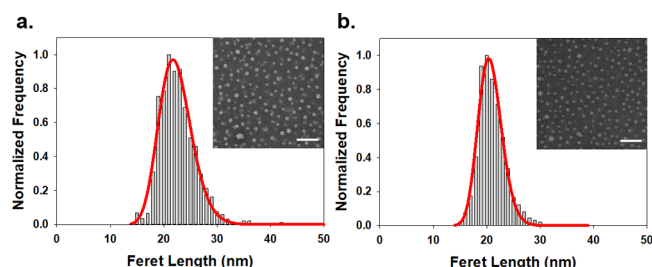


Figure 5. TEM analysis of PS-*b*-PEO NPs encapsulating (a) QDs and (b) SPIONs synthesized via EM-NP at an organic flow rate of 12.7 mL h⁻¹ and an applied voltage of -2500 V. Size distributions (histogram bin size: 1 nm) for the loaded NPs and the corresponding log-normal fits (red). Insets: TEM images; scale bar = 100 nm.

for with SPIONs, close to the $\langle L_F \rangle$ of 19 nm measured for empty PS-*b*-PEO NPs synthesized using the same process parameters (i.e., BCP concentration, voltage, and flow rate). In contrast, the maximum L_F for loaded PS-*b*-PEO composites was much larger (54.6 nm for QDs and 38.1 nm for SPIONs) than the empty PS-*b*-PEO NPs (Max L_F = 30.3 nm). Furthermore, mean $\langle L_F \rangle$ values for the loaded PS-*b*-PEO NPs synthesized via EM-NP were ~ 9 nm (QD) and ~ 6 nm (SPION) smaller than those obtained for comparable PS-*b*-PEO NPs synthesized via the sonication method used in our earlier work.⁴¹ Finally, conventional synthesis methods resulted in broader particle size distributions and the formation of elongated morphologies that were never observed here.⁴¹

The slight increase in mean size observed could result from PS block stretching on the addition of hydrophobic encapsulants, as has been observed previously.⁵ The increase in the maximum L_F is associated with nanocomposites containing multiple inorganic NPs and most likely reflects the difference between τ_{ng} and τ_{agg} . In FNP, the key to high encapsulation and product uniformity is to ensure τ_{agg} , the time scale of BCP aggregation is approximately equal to τ_{ng} , the hydrophobic cargo nucleation and growth time. Although characterizing τ_{agg} for PS-*b*-PEO and τ_{ng} for QDs and SPIONs is beyond the scope of this paper, our results suggest that reducing τ_{agg} relative to τ_{ng} by changing the solvent quality or increasing the inorganic NP concentration could improve product uniformity by reducing the number of empty polymer NPs. Nonetheless, EM-NP yielded highly monodisperse PS-*b*-PEO composites with roughly 50–70% of the composites containing at least 1 inorganic NP.

Finally, to demonstrate the suitability of EM-NP for processing delicate cargo, we measured the fluorescence intensity of PS-*b*-PEO NPs encapsulating QDs over the course of 7 days (Figure 6). QDs are sensitive to environmental conditions, particularly in aqueous environments,^{17,47} where they can undergo photo-oxidation and loss of stabilizing ligands. After the first 24 h, fluorescence intensity diminished by $\sim 20\%$ (i.e., declined to 80% of that originally obtained immediately after the synthesis); however, fluorescence was stable over the remaining 6 days of observation. These results suggest that BCPs adequately stabilize QDs against environmental assaults and that initial fluorescence declines may result from the EM-NP process.

CONCLUSIONS

EM-NP provides a robust platform for producing BCP NPs and functional nanocomposites via the FNP mechanism. EM-

Table 3. Size Characteristics of PS–PEO NPs Encapsulating QDs and SPIONs^a

encapsulants	min L_F (nm)		max L_F (nm)		mode L_F (nm)		mean L_F^+ (nm)		PD _{eff}	
	empty	loaded	empty	loaded	empty	loaded	empty	loaded	empty	loaded
QDs	14.6	13.3	24.1	54.6	17.7	21.7	18.1 ^{+2.4} _{-2.1}	22.3 ^{+3.3} _{-2.9}	0.12	0.14
SPIONs	13.9	13.7	24.4	38.1	16.6	20.4	17.0 ^{+2.2} _{-1.9}	20.7 ^{+2.3} _{-2.1}	0.12	0.11
no NPs	13.1	N/A	30.3	N/A	18.5	N/A	19.0 ^{+2.6} _{-2.3}	N/A	0.13	N/A

^a L_F = Feret length. +, -: the interval defined by the upper and lower bounds on $\langle L_F \rangle$ contains 68% of the particles. PD_{eff} = $\sqrt{(+dev)(-dev)}/\langle L_F \rangle$

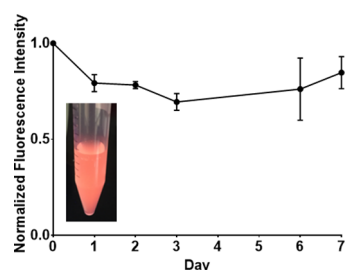


Figure 6. Fluorescence intensity of PS–PEO composites encapsulating QDs normalized to the initial fluorescence intensity observed immediately after the synthesis.

NP is, however, fundamentally different from other FNP platforms in that rapid mixing is achieved by EHD mixing and instability of the interface induced by electrical stresses, instead of turbulent flow. Because mixing is primarily dependent on the applied voltage, rapid mixing can be achieved at flow rates significantly lower than those used in most FNP mixers ($\sim \text{mL h}^{-1}$ compared to mL min^{-1}). Characterizing the exact time scales, especially τ_{mix} at different voltage settings, is beyond the scope of this paper. Further in-depth investigation to better understand and control the time scales of mixing, BCP aggregation, and hydrophobic cargo nucleation and growth will help extend the reach of this technology. The current results demonstrate that homogeneous aggregation kinetics are easily obtained via EM-NP. Furthermore, in the current experiments, NP size and polydispersity are relatively insensitive to changes in flow rate and consistent with prior FNP results, independent of BCP concentration.⁸ We acknowledge that the current study only used one molecular weight for each of the two BCPs investigated. To better understand the strengths and limitations of the EM-NP process, we are currently investigating a wider range of BCPs and molecular weights to evaluate the effect of these variables on particle formation via EM-NP.

The ability to form highly monodisperse NPs using a method that is essentially independent of flow rate provides a desirable alternative for controlled, lower volume processes and encapsulation of delicate cargo. Ideally, encapsulation processes should provide high efficiency, while preserving functionality. For example, hydrophobic encapsulants employed in bioimaging and drug delivery comprise high value components that may be sensitive to processing conditions. Here, EM-NP was used to encapsulate inorganic NPs, including QDs and SPIONs, used in biological imaging. QDs in particular represent a delicate cargo in that they are extremely sensitive to environmental conditions. In the EM-NP process, fluorescence of encapsulated QDs declined by 20% within 24 h but maintained that fluorescence level for the remainder of the 7 day test.

Equally important are inline quality and process control, which may be more difficult to achieve if large flow rates are

used. Because the success of EM-NP is not heavily dependent on flow rate, more controlled production may be possible. Further, lower flow rates need not limit scale. Whereas product throughputs from units used in this study were much lower than those of conventional FNP platforms, scale up of individual units should be possible by increasing the flow through the electrified capillary with concomitant increases in power supply, by multiplexing using an array of needles, or by turning the system into a continuous process. Thus, EM-NP provides a promising alternative route to synthesize mono-disperse polymer nanocomposites with little flow rate dependence that has potential to reach commercial scales.

■ ASSOCIATED CONTENT

📄 Supporting Information

The Supporting Information is available free of charge on the ACS Publications website at DOI: 10.1021/acsapm.8b00206.

Lognormal fits and size distribution analysis methods of experiments; supplemental figures and tables (PDF)

■ AUTHOR INFORMATION

Corresponding Authors

*E-mail: wyslouzil.1@osu.edu.

*E-mail: winter.63@osu.edu.

ORCID

Barbara E. Wyslouzil: 0000-0001-9763-5990

Jessica O. Winter: 0000-0002-5370-0137

Author Contributions

||B.E.W. and J.O.W. contributed equally.

Notes

The authors declare the following competing financial interest(s): Dr. Winter is a founder and equity holder in Core Quantum Technologies a company creating quantum dot reagents for cancer detection.

■ ACKNOWLEDGMENTS

This work was funded by the National Science Foundation under Grants CMMI-1344567 and DMR-1206745.

■ REFERENCES

- (1) Ladj, R.; Bitar, A.; Eissa, M. M.; Fessi, H.; Mugnier, Y.; Le Dantec, R.; Elaissari, A. Polymer encapsulation of inorganic nanoparticles for biomedical applications. *Int. J. Pharm.* **2013**, *458*, 230–241.
- (2) Prateek, T. V. K.; Gupta, R. K.; et al. Recent progress on ferroelectric polymer-based nanocomposites for high energy density capacitors: synthesis, dielectric properties, and future aspects. *Chem. Rev.* **2016**, *116*, 4260–4317.
- (3) Hayward, R. C.; Pochan, D. J. Tailored assemblies of block copolymers in solution: it is all about the process. *Macromolecules* **2010**, *43*, 3577–3584.
- (4) Li, J.; Li, X.; Ni, X.; Wang, X.; Li, H.; Leong, K. W. Self-assembled supramolecular hydrogels formed by biodegradable PEO–

PHB-PEO triblock copolymers and α -cyclodextrin for controlled drug delivery. *Biomaterials* **2006**, *27*, 4132–4140.

(5) Mai, Y.; Eisenberg, A. Self-assembly of block copolymers. *Chem. Soc. Rev.* **2012**, *41*, 5969–5985.

(6) Meng, H.; Hu, J. A brief review of stimulus-active polymers responsive to thermal, light, magnetic, electric, and water/solvent stimuli. *J. Intell. Mater. Syst. Struct.* **2010**, *21*, 859–885.

(7) Murday, J. S.; Siegel, R. W.; Stein, J.; Wright, J. F. Translational nanomedicine: status assessment and opportunities. *Nanomedicine* **2009**, *5*, 251–273.

(8) Johnson, B. K.; Prud'homme, R. K. Mechanism for rapid self-assembly of block copolymer nanoparticles. *Phys. Rev. Lett.* **2003**, *91*, 118302.

(9) Zhang, L.; Eisenberg, A. Thermodynamic vs kinetic aspects in the formation and morphological transitions of crew-cut aggregates produced by self-assembly of polystyrene-*b*-poly (acrylic acid) block copolymers in dilute solution. *Macromolecules* **1999**, *32*, 2239–2249.

(10) Marsden, H. R.; Gabrielli, L.; Kros, A. Rapid preparation of polymersomes by a water addition/solvent evaporation method. *Polym. Chem.* **2010**, *1*, 1512–1518.

(11) Saad, W. S.; Prud'homme, R. K. Principles of nanoparticle formation by flash nanoprecipitation. *Nano Today* **2016**, *11*, 212–227.

(12) Akbulut, M.; Ginart, P.; Gindy, M. E.; Theriault, C.; Chin, K. H.; Soboyejo, W.; Prud'homme, R. K. Generic Method of Preparing Multifunctional Fluorescent Nanoparticles Using Flash NanoPrecipitation. *Adv. Funct. Mater.* **2009**, *19*, 718–725.

(13) Han, J.; Zhu, Z.; Qian, H.; Wohl, A. R.; Beaman, C. J.; Hoyer, T. R.; Macosko, C. W. A simple confined impingement jets mixer for flash nanoprecipitation. *J. Pharm. Sci.* **2012**, *101*, 4018.

(14) Ding, S.; Anton, N.; Vandamme, T. F.; Serra, C. A. Microfluidic nanoprecipitation systems for preparing pure drug or polymeric drug loaded nanoparticles: an overview. *Expert Opin. Drug Delivery* **2016**, *13*, 1447–1460.

(15) Lu, Y.; Chowdhury, D.; Vladislavjević, G. T.; Koutroumanis, K.; Georgiadou, S. Production of fluconazole-Loaded polymeric micelles using membrane and microfluidic dispersion devices. *Membranes* **2016**, *6*, 29.

(16) DePaoli, D. W.; Tsouris, C.; Hu, M. Z. C. EHD micromixing reactor for particle synthesis. *Powder Technol.* **2003**, *135*, 302–309.

(17) Aldana, J.; Wang, Y. A.; Peng, X. Photochemical instability of CdSe nanocrystals coated by hydrophilic thiols. *J. Am. Chem. Soc.* **2001**, *123*, 8844–50.

(18) Melcher, J. R.; Taylor, G. I. Electrohydrodynamics: a review of the role of interfacial shear stresses. *Annu. Rev. Fluid Mech.* **1969**, *1*, 111–146.

(19) Taylor, G. Disintegration of Water Drops in an Electric Field. *Proc. R. Soc. London, A* **1964**, *280*, 383–397.

(20) Jaworek, A.; Krupa, A. *Main modes of electrohydrodynamic spraying of liquids*, Third International Conference on Multiphase Flow, Lyon, France, 1998.

(21) Duong, A. D.; Ruan, G.; Mahajan, K.; Winter, J. O.; Wyslouzil, B. E. Scalable, Semicontinuous Production of Micelles Encapsulating Nanoparticles via Electrospray. *Langmuir* **2014**, *30*, 3939–3948.

(22) Sridhar, R.; Ramakrishna, S. Electrospayed nanoparticles for drug delivery and pharmaceutical applications. *Biomater* **2013**, *3*, e24281.

(23) Wu, Y.; Fei, Z.; Lee, L. J.; Wyslouzil, B. E. Coaxial Electrohydrodynamic Spraying of Plasmid DNA/Polyethylenimine (PEI) Polyplexes for Enhanced Nonviral Gene Delivery. *Biotechnol. Bioeng.* **2009**, *105*, 834–841.

(24) Almería, B.; Deng, W.; Fahmy, T. M.; Gomez, A. Controlling the morphology of electrospray-generated PLGA microparticles for drug delivery. *J. Colloid Interface Sci.* **2010**, *343*, 125–133.

(25) Sato, M.; Saito, M.; Hatori, T. Emulsification and size control of insulating and/or viscous liquids in liquid-liquid systems by electrostatic dispersion. *J. Colloid Interface Sci.* **1993**, *156*, 504–507.

(26) Sato, M.; Morita, N.; Kuroiwa, I.; Ohshima, T.; Urashima, K. Dielectric Liquid-in-Liquid Dispersion by Applying Pulsed Voltage. *IEEE Trans. Dielectr. Electr. Insul.* **2009**, *16*, 391–395.

(27) Sato, M.; Kuroiwa, I.; Ohshima, T.; Urashima, K. Production of Nano-silica Particles in Liquid-liquid System by Pulsed Voltage Application. *IEEE Trans. Dielectr. Electr. Insul.* **2009**, *16*, 320–324.

(28) Tsouris, C.; Depaoli, D. W.; Feng, J. Q.; Basaran, O. A.; Scott, T. C. Electrostatic Spraying of Nonconductive Fluids into Conductive Fluids. *AIChE J.* **1994**, *40*, 1920–1923.

(29) Tsouris, C.; DePaoli, D. W.; Feng, J. Q.; Scott, T. C. Experimental investigation of electrostatic dispersion of nonconductive fluids into conductive fluids. *Ind. Eng. Chem. Res.* **1995**, *34*, 1394–1403.

(30) Atten, P. Electrohydrodynamic instability and motion induced by injected space charge in insulating liquids. *IEEE Trans. Dielectr. Electr. Insul.* **1996**, *3*, 1–17.

(31) Feng, H.; Wong, T. N.; Che, Z.; Marcos. Chaotic micromixer utilizing electro-osmosis and induced charge electro-osmosis in eccentric annulus. *Phys. Fluids* **2016**, *28*, 062003.

(32) Hassen, W.; Elkhazen, M. I.; Traore, P.; Borjini, M. N. Charge injection in horizontal eccentric annuli filled with a dielectric liquid. *European Journal of Mechanics-B/Fluids* **2018**, *72*, 691–700.

(33) Atten, P.; Elouadie, L. EHD convection in a dielectric liquid subjected to unipolar injection: coaxial wire/cylinder geometry. *J. Electrostat.* **1995**, *34*, 279–297.

(34) Gross, M. J.; Porter, J. E. Electrically induced convection in dielectric liquids. *Nature* **1966**, *212*, 1343–1345.

(35) Stuetzer, O. M. Ion drag pumps. *J. Appl. Phys.* **1960**, *31*, 136–146.

(36) Sato, M.; Hatori, T.; Saito, M. Experimental investigation of droplet formation mechanisms by electrostatic dispersion in a liquid-liquid system. *IEEE Trans. Ind. Appl.* **1997**, *33*, 1527–1534.

(37) Gindy, M. E.; Panagiotopoulos, A. Z.; Prud'homme, R. K. Composite block copolymer stabilized nanoparticles: Simultaneous encapsulation of organic actives and inorganic nanostructures. *Langmuir* **2008**, *24*, 83–90.

(38) Nabar, G. M.; Mahajan, K. D.; Calhoun, M. A.; Duong, A. D.; Souva, M. S.; Xu, J.; Czeisler, C.; Puduvali, V. K.; Otero, J. J.; Wyslouzil, B. E.; Winter, J. O. Micelle-templated, poly(lactic-co-glycolic acid) nanoparticles for hydrophobic drug delivery. *Int. J. Nanomed.* **2018**, *13*, 351–366.

(39) Johnson, B. K.; Prud'homme, R. K. Flash NanoPrecipitation of organic actives and block copolymers using a confined impinging jets mixer. *Aust. J. Chem.* **2003**, *56*, 1021–1024.

(40) Wang, M.; Xu, Y.; Liu, Y.; Gu, K.; Tan, J.; Shi, P.; Yang, D.; Guo, Z.; Zhu, W.; Guo, X.; Cohen Stuart, M. A. Morphology Tuning of Aggregation-Induced Emission Probes by Flash Nanoprecipitation: Shape and Size Effects on in Vivo Imaging. *ACS Appl. Mater. Interfaces* **2018**, *10*, 25186–25193.

(41) Nabar, G. M.; Winter, J. O.; Wyslouzil, B. E. Nanoparticle packing within block copolymer micelles prepared by the interfacial instability method. *Soft Matter* **2018**, *14*, 3324–3335.

(42) Souva, M. S.; Nabar, G. M.; Winter, J. O.; Wyslouzil, B. E. Morphology of block copolymer micelles formed via electrospray enabled interfacial instability. *J. Colloid Interface Sci.* **2018**, *512*, 411–418.

(43) Zhu, Z.; Anacker, J. L.; Ji, S.; Hoyer, T. R.; Macosko, C. W.; Prud'homme, R. K. Formation of Block Copolymer-Protected Nanoparticles via Reactive Impingement Mixing. *Langmuir* **2007**, *23*, 10499–10504.

(44) Chen, T.; Hynninen, A.-P.; Prud'homme, R. K.; Kevrekidis, I. G.; Panagiotopoulos, A. Z. Coarse-grained simulations of rapid assembly kinetics for polystyrene-*b*-poly (ethylene oxide) copolymers in aqueous solutions. *J. Phys. Chem. B* **2008**, *112*, 16357–16366.

(45) Morkved, T. L.; Lu, M.; Urbas, A. M.; Ehrichs, E. E.; Jaeger, H. M.; Mansky, P.; Russell, T. P. Local control of microdomain orientation in diblock copolymer thin films with electric fields. *Science* **1996**, *273*, 931–933.

(46) Zhu, J.; Hayward, R. C. Spontaneous generation of amphiphilic block copolymer micelles with multiple morphologies through interfacial instabilities. *J. Am. Chem. Soc.* **2008**, *130*, 7496–7502.

(47) Aldana, J.; Lavelle, N.; Wang, Y.; Peng, X. Size-Dependent Dissociation pH of Thiolate Ligands from Cadmium Chalcogenide Nanocrystals. *J. Am. Chem. Soc.* **2005**, *127*, 2496–2504.